Inversion of GPS data for spatially variable slip-rate on the San Andreas Fault near Parkfield, CA

J. R. Murray, P. Segall, P. Cervelli,

Department of Geophysics, Stanford University, Stanford, CA

W. Prescott and J. Svarc

United States Geological Survey, Menlo Park, CA

Abstract. We analyze GPS data collected from 1991-1998 at 35 sites near the Parkfield segment of the San Andreas Fault. Inverting the resultant site velocities for the distribution of interseismic slip-rate on the San Andreas reveals an area of low slip-rate on the fault extending from between Middle Mountain and Carr Hill to southeast of Gold Hill. This slip-rate pattern is similar to that found by *Harris and Segall* [1987] using trilateration data collected between 1966 and 1984. We infer a deep slip-rate (33 mm/yr) and depth of the transition between seismogenic and non-seismogenic slip (14 km) that agree better with independent geologic evidence than those found in the 1987 study. In contrast to *Harris and Segall* [1987], we find no evidence of fault-normal contraction.

Introduction

The Parkfield segment of the San Andreas fault (figure 1) forms a transition between the creeping segment to the northwest [*Savage and Burford*, 1971], and the locked section that last ruptured in the *M* 8 1857 Fort Tejon earthquake [*Sieh*, 1978] to the southeast. At least 5 historic earthquakes of ∼*M* 6 have occurred in this area, in 1881, 1901, 1922, 1934, and 1966, although other San Andreas events may have occurred near Parkfield in 1877 and 1908 [*Toppozada*, 1992]. Seismograms from the 1922, 1934, and 1966 events indicate that these earthquakes had similar hypocenter, moment, and focal mechanism [*Bakun and McEvilly*, 1984]. These authors described the Parkfield events as "characteristic" and predicted the next earthquake would occur in 1988 ± 5 years. However, to date the most recent ∼*M* 6 event here was in 1966. Others have noted the Parkfield earthquakes are not strictly characteristic [e. g., see *Roeloffs and Langbein*, 1994]. *Segall and Du* [1993] inferred from geodetic data that the 1966 event ruptured further to the southeast and may have had a larger moment than the 1934 earthquake.

Harris and Segall [1987] inverted trilateration data collected between 1966 and 1984 for the distribution of slip-rate on the Parkfield segment of the San Andreas. They found a "locked patch" extending NW from the 1857 rupture zone to the area below Middle Mountain. This patch of low slip-rates roughly coincides with the aftershock zone from the 1966 earthquake. *Harris and Segall* [1987] also found that a systematic misfit between data and model prediction could

be reduced by including a small component of fault-normal shortening. More recent data [*Dong*, 1993; *Shen and Jackson*, 1993], however, do not show this shortening.

The U. S. Geological Survey has used the Global Positioning System (GPS) to make repeated position measurements of sites in the Parkfield area since the late 1980s [*Davis et al.*, 1989]. These data are methodologically and temporally independent of the earlier trilateration data. In our study, we assess whether the inferred locked patch persists by inverting the GPS data for interseismic slip-rate distribution.

Data collection and processing

Between 1991 and 1998 the USGS conducted 15 GPS campaigns involving 35 sites in the Parkfield area. We processed these data with GIPSY-OASIS II software using a bias-fixed, precise point positioning technique [*Gregorius*, 1996; *Zumberge et al.*, 1997]. We incorporated the National Geodetic Survey (NGS) phase center calibrations to correct for multiple antenna types. We treated the wet zenith troposphere delay as a stochastic random walk parameter with a tropospheric drift parameter of 9.5 x 10^{-8} km/$\sqrt{sec}$ [*Gregorius*, 1996]. Analysis of continuous GPS measurements in the Parkfield area showed that this value minimizes the short-term scatter in the daily solutions. We used non-fiducial satellite orbits and clock corrections produced by NASA's Jet Propulsion Laboratory (JPL). After processing, we applied JPL's date-specific Helmert transformations to transform the position solutions from each day's nonfiducial reference frame to an ITRF96 frame.

Assuming steady state deformation, we solved for constant station velocities using weighted least squares (figure 1). The formal position errors were scaled so that the mean square error of the velocity estimate was approximately one. Typical rms values about the best fitting lines are 6.4 mm (east), 5.8 mm (north), and 19 mm (up).

Inversion

We assumed that the surface displacements observed in the Parkfield area arise from right lateral strike slip along the San Andreas fault, which we modeled as a dislocation in a homogeneous, linear, elastic half-space. Discretizing the model fault into a grid of uniformly sized blocks (3 km long by 2 km high) and taking the time derivative of *Okada's* [1985] expressions, we expressed the surface velocities as the sum of contributions from slip across each of the blocks.

For a specified fault geometry, the inversion for slip-rate is linear. The orientation of the San Andreas fault near
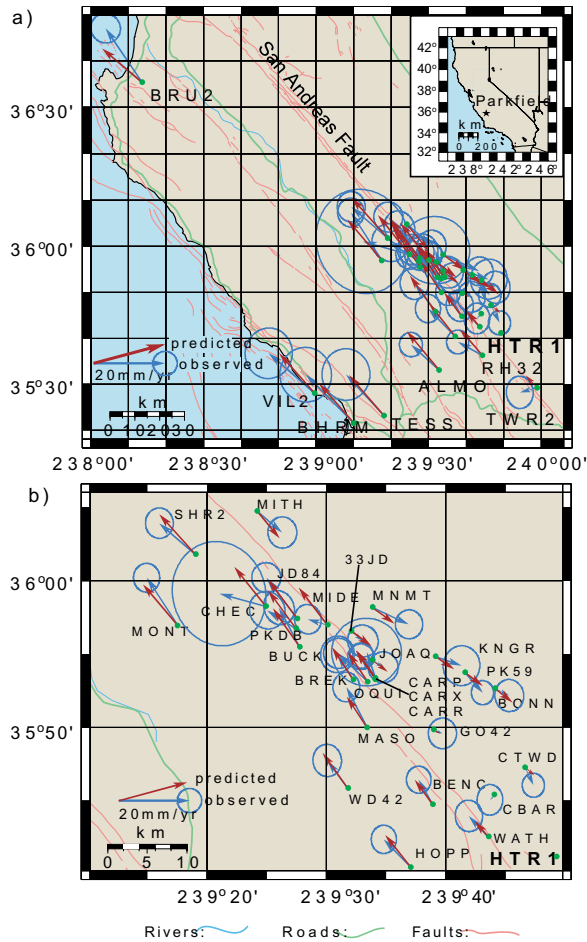
a)

b)

Figure 1. GPS stations used in this study. Observed velocities with 95% confidence ellipses and predicted velocities based on results of non-negative least squares (NNLS) inversion. a) Overview. b) Close-up of stations near Parkfield, CA. Town of Parkfield is ∼ 1.5 km north of station CARR. Velocities plotted relative to that of station HTR1.

Parkfield is known from geologic mapping [*Lienkaemper and Brown*, 1985; *Sims*, 1990] and the spatial distribution of microseismicity [*Eaton et al.*, 1970; *Eberhart-Phillips and Michael*, 1993]. The epicenter of the 1966 earthquake (which nucleated below Middle Mountain), its aftershocks [*Eaton et al.*, 1970], and its inferred rupture area [*Segall and Du*, 1993] define the Parkfield segment. Like that used by *Harris and Segall* [1987], the model fault plane is vertical and 36 km long. It strikes N41°W and extends from a point ∼6 km northwest of Middle Mountain to ∼11.5 km southeast of Gold Hill. We appended a block 100 km long and of depth equal to that of the model Parkfield plane on either side of the gridded fault to simulate the effect of the neighboring creeping and locked segments. A block 1000 km long and wide was centered below the Parkfield plane to represent deep slip and far-field plate motion.

We constrained the slip-rate of the 12 shallowest blocks on the gridded plane to 24 mm/yr in the NW, decreasing to 4 mm/yr in the SE based on near-fault data from creep meters, alinement arrays, and short aperture geodetic networks [see *Harris and Segall*, 1987]. While these data span an earlier time period than the GPS data, they should reflect the first-order distribution of shallow slip-rate. We constrained the slip-rate on the creeping section to 25 mm/yr [*Lisowski*

and Prescott, 1981]. These 13 a priori data were assigned much smaller uncertainties than the GPS measurements.

We assumed a spatially smooth slip-rate distribution as measured by a finite difference Laplacian operator [e.g., *Harris and Segall*, 1987]. Using damped least squares (DLS), we simultaneously minimized the L_2 norm of the model (which represents the roughness of the slip-rate distribution) and the L_2 norm of the weighted residuals. A damping parameter, ε, controls the relative emphasis put on minimizing the model roughness (high ε) versus keeping the misfit small (low ε) [e.g., *Du et al.*, 1992]. We used cross validation (CV) to choose an optimal value for ε [*Wahba*, 1990]. For each value of ε, a series of slip-rate estimates was found, each with one datum omitted. The residual between an omitted datum and that predicted by the model is the "cross-validation residual". The "cross validation sum of squares" (CVSS) is the sum of these squared residuals for a given ε. The optimal value of ε corresponds to the smallest CVSS. An estimate with too little smoothing will model noise, preventing it from adequately predicting the omitted datum. Estimates with too much smoothing will have greater misfit. While CV is objective, it is computationally intensive and requires that one know the data correlations.

Another criterion we applied when choosing ε was that slip must be everywhere right lateral (positive). This tended to result in higher values for ε and, thus, reduced resolution. *Du et al.* [1992] showed that imposing a positivity constraint using non-negative least squares (NNLS) [*Lawson and Hanson*, 1974] improves resolution, and we present results using this method below. For the NNLS inversions, we treated the smoothing constraints as pseudo-observations, so minimizing the residual between observed and predicted data simultaneously optimized data fit and minimized model roughness [*Segall and Du*, 1993]. This results in the following equations:

$$\begin{bmatrix} \mathbf{d} \\ \mathbf{0} \end{bmatrix} = \begin{bmatrix} \mathbf{G} \\ \mathbf{T} \end{bmatrix} \dot{\mathbf{s}} + \epsilon \qquad (1)$$

where $\mathbf{d}$ is a vector of station velocities, $\dot{\mathbf{s}}$ a vector of slip-rates on the discretized fault, and $\mathbf{G}$ a matrix of coefficients relating the two. $\mathbf{T}$ is the Laplacian smoothing matrix, and
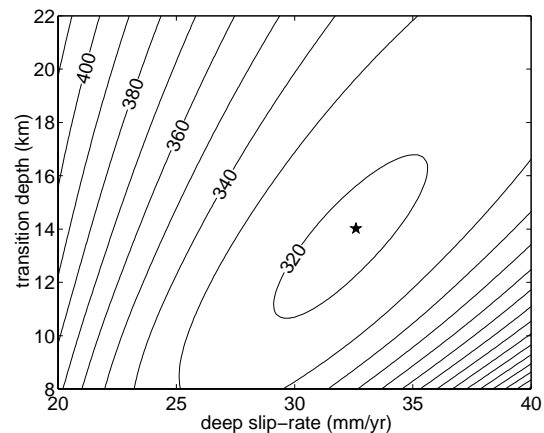

Figure 2. Contours of CVSS for DLS inversions using optimal ε for a range of transition depths and deep slip-rates. Contours are interpolated between the transition depths marked on the y-axis. Optimal transition depth/deep slip-rate pair (star) is 14 km and 32.6 mm/yr.
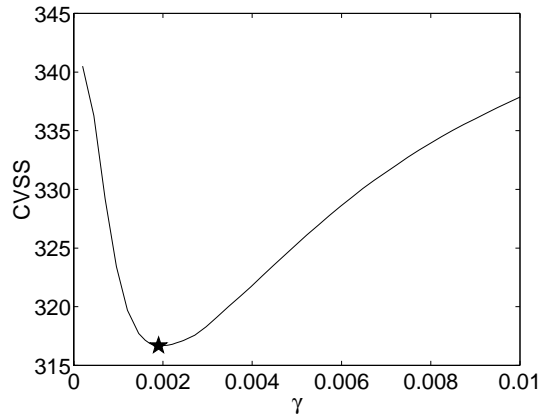
Figure 3. CVSS as a function of γ for NNLS inversions. Minimum CVSS (star) occurs for $\gamma = 0.0019$. Transition depth = 14 km; deep slip-rate = 32.6 mm/yr.

$\epsilon \sim N(0, \Sigma_d)$. The data covariance matrix, Σ_d, is given by:

$$\Sigma_d = \begin{bmatrix} \Sigma_{geod} & 0 \\ 0 & \gamma^2 I \end{bmatrix} \qquad (2)$$

where Σ_{geod}, is the covariance matrix of the velocity solution and surface constraints, and γ is a damping parameter chosen by CV. Smaller values of γ lead to smoother solutions.

Results

There is a trade-off in the relationship between the deep slip-rate below the Parkfield plane and the transition depth from episodic to steady slip. *Harris and Segall* [1987] found that as transition depth ranged from 14 - 22 km, the estimated deep slip-rate varied from 25.5 - 32.7 mm/yr.

In order to determine the optimal combination of transition depth and deep slip-rate, we compared the minimum CVSS (which corresponds to the optimal amount of smoothing) for slip-rate distributions found using DLS spanning a range of depths and constrained deep slip-rates (figure 2). NNLS is was too computationally intensive for finding the minimum CVSS for this large number of depth / deep slip-rate pairs. The minimum CVSS occurred for a transition depth of 14 km and a deep slip-rate of 32.6 mm/yr. This rate is higher than that found by *Harris and Segall* for a transition depth of 14 km but is more in keeping with geologic estimates of $\sim 33.9 \pm 2.9$ mm/yr [*Sieh and Jahns*, 1984]. The 1966 aftershocks and background seismicity extend to depths of ~ 14 km [*Eaton et al.*, 1970; *Eberhart-Phillips and Michael*, 1993], implying that slip-rate transients extend to this depth. We constrained the transition depth and deep slip-rate to 14 km and 32.6 mm/yr in the following inversions.

For the NNLS inversions, cross validation yielded an estimate of $\gamma = 0.0019$ (figure 3). The corresponding slip-rate distribution (figure 4) shows a zone of low slip-rate extending northwest to the area between Carr Hill and Middle Mountain. The slip-rates are similar to, but slightly lower than, those found using DLS, and the fit to the data is not discernibly different.

Overall, the estimated slip-rate distribution fits the data well (figure 1). There is obvious misfit at stations BRU2, MIDE, and TWR2. The predicted velocities of ALMO,

PKDB, and RH32 narrowly exceed the observations at 95% confidence. The misfit at TWR2 may arise in part from the fault model's failure to account for the right step in the fault trace near the town of Cholame. One should note that the uncertainties in the data do not reflect unmodeled noise sources such as benchmark instability, although preliminary analysis suggests that this is not a limiting factor in the computed velocities. The area of greatest misfit is at the northwest end of the Parkfield plane. This may be due to unstable benchmarks, distributed deformation, or inaccurate creep constraints. Inclusion of additional near-fault geodetic data with uncertainties that accurately reflect the effect of local site instabilities will help clarify this issue. There is no systematic misfit that would suggest fault normal contraction.

Discussion

The slip-rate distributions we have estimated based on GPS data are, for the southeastern half of the model plane, quite similar to those found by *Harris and Segall* [1987] using a data set that was different in both collection method and temporal coverage. This suggests that certain large-scale features of the slip-rate distribution at depth in the Parkfield area are fairly constant over decadal time scales. However, the low slip-rate zone we modeled does not extend as far northwest, and the slip-rates we found are slightly higher than those of *Harris and Segall's* study. There are several things one must consider when attempting to interpret these observations.

First, *Harris and Segall* allowed their slip-rate distribution to include slightly negative values. This may in part account for our solution's having an overall higher slip-rate. Furthermore, inspection of the resolving kernels for our inversion, which show how slip-rate on the fault is resolved spatially, indicates that only features with spatial extent larger than ~ 12 km are meaningful. The along strike distance between the 10 mm/yr contour 6-8 km below Middle Mountain in the two studies is 7.5 km. Thus, the difference is probably below the resolution of the data.

Several authors [*Gwyther et al.*, 1996; *Langbein et al.*, 1999; *Nadeau and McEvilly*, 1999; *Gao et al.*, 2000] have presented evidence for a change in slip-rate in the area between Carr Hill and Middle Mountain in the early to mid 1990s. Therefore, our model may reflect a higher rate of aseismic slip during the time the GPS data were collected (1991-1998) in comparison to that covered by the trilateration data (1966-1984). In the early 1990's there was a series
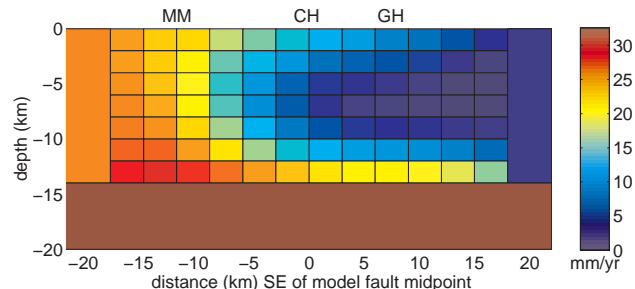

Figure 4. Slip distribution found using NNLS with $\gamma = 0.0019$, transition depth = 14 km, deep slip-rate = 32.6 mm/yr. MM = Middle Mountain, CH = Carr Hill, GH = Gold Hill.

of $M{>}4$ earthquakes in the Middle Mountain area. Based on estimates of the moment, rupture area, and slip in these events [*Fletcher and Spudich*, 1998], we conclude that it is unlikely these events alone account for the differences in slip-rate distribution. Finally, one should note that the absence of GPS sites further than 5 km perpendicular to the fault near Middle Mountain particularly limits the resolution of slip-rate below 5 km on this part of the fault plane.

Based on these considerations, we conclude that our model and that of *Harris and Segall* [1987] are qualitatively similar. The earlier study found low slip-rate on the portion of the 1966 rupture plane closer to the earthquake hypocenter. The results of our inversions clearly demonstrate the persistence of a slip-rate deficit on the southeastern end of the plane. Interestingly, the area of lowest slip-rate we image coincides with the area found by the inversion of geodetic data to have the highest slip during the 1966 earthquake [*Segall and Du*, 1993].

Conclusions

Using GPS data collected between 1991 and 1998, we inferred the distribution of fault slip-rate at depth on the Parkfield segment of the San Andreas Fault. The data were best fit with a transition from transient to steady slip at a depth of 14 km and with a deep slip-rate of 32.6 mm/yr, in good agreement with independent seismic and geologic data. Inversions strongly supported the presence of a low slip-rate patch at depth on the Parkfield segment. The persistence of low slip-rate implies that, over the time spanned by the GPS data, strain has continued to build in this region. *Segall and Harris* [1986] predicted that the strain released in the 1966 earthquake would have recovered by 1995. The fact that the earthquake has yet to occur raises questions about the characteristic earthquake model used in the original forecasts.

References

Bakun, W. H., and T. V. McEvilly, Recurrence models and Parkfield, California, earthquakes, *J. Geophys. Res., 89,* 3051-3058, 1984.

Davis, J. L., W. H. Prescott, J. L. Svarc, and K. J. Wendt, Assessment of Global Positioning System measurements for studies of crustal deformation, *J. Geophys. Res., 94,* 13,635-13,650, 1989.

Dong, D., The horizontal velocity field in Southern California from a combination of terrestrial and space-geodetic data, Ph.D. thesis, 157 pp., M.I.T., Cambridge, Mass., Sept. 1993.

Du, Y., A. Aydin, and P. Segall, Comparison of various inversion techniques as applied to the determination of a geophysical deformation model for the 1983 Borah Peak earthquake, *Bull. Seismol. Soc. Am., 82,* 4, 1840-1866, 1992.

Eaton, J. P., M. E. O'Neill, and J. N. Murdock, Aftershocks of the 1966 Parkfield-Cholame, California, earthquake: A detailed study, *Bull. Seismol. Soc. Am., 60,* 4, 1151-1197, 1970.

Eberhart-Phillips, D., and A. J. Michael, Three-dimensional velocity structure, seismicity, and fault structure in the Parkfield region, central California, *J. Geophys. Res., 98,* 15,737-15,758, 1993.

Fletcher, J. B. and P. Spudich, Rupture characteristics of the three $M \sim 4.7$ (1992-1994) Parkfield earthquakes, *J. Geophys. Res., 103,* 835-854, 1998.

Gao, S., P. G. Silver, and A. T. Linde, A comprehensive analysis of deformation data at Parkfield, CA: Detection of a long-term strain transient, *J. Geophys. Res., 105,* 2955-2967, 2000.

Gregorius, T. GIPSY-OASIS II: How it Works, (self-published), Univ. of Newcastle upon Tyne, Newcastle, England, U.K., 1996.

Gwyther, R. L., M. T. Gladwin, M. Mee, and R. H. G. Hart, Anomalous shear strain at Parkfield during 1993-94, *Geophys. Res. Lett., 23,* 18, 2425-2428, 1996.

Harris, R. A., and P. Segall, Detection of a locked zone at depth on the Parkfield, California, segment of the San Andreas fault, *J. Geophys. Res., 92,* 7945-7962, 1987.

Langbein, J., R. L. Gwyther, R. H. G. Hart, and M. T. Gladwin, Slip-rate increase at Parkfield in 1993 detected by high-precision EDM and borehole tensor strainmeters, *Geophys. Res. Lett., 26,* 16, 2529-2532, 1999.

Lawson, C. L., and R. J. Hanson, *Solving Least Squares Problems,* Prentice-Hall, Englewood Cliffs, New Jersey, 1974.

Lienkaemper, J. J. and R. D. Brown, Map of faulting accompanying the 1966 Parkfield, California, earthquake, *U.S. Geol. Surv. Open File Rep.,* 85-661, 1985.

Lisowski, M., and W. H. Prescott, Short-range distance measurements along the San Andreas fault system in central California, 1975 to 1979, *Bull. Seismol. Soc. Am., 71,* 5, 1607-1624, 1981.

Nadeau, R. M., and T. V. McEvilly, Fault slip rates at depth from recurrence intervals of repeating microearthquakes, *Science, 285,* 718-721, 1999.

Okada, Y., Surface deformation due to shear and tensile faults in a half-space, *Bull. Seismol. Soc. Am., 75,* 4, 1135-1154, 1985.

Roeloffs, E., and J. Langbein, The earthquake prediction experiment at Parkfield, California, *Rev. Geophys., 32,* 3, 315-336, 1994.

Savage, J. C., and R. O. Burford, Discussion of paper by C. H. Scholz and T. J. Fitch, 'Strain accumulation along the San Andreas fault', *J. Geophys. Res., 76,* 6469-6479, 1971.

Segall, P., and Y. Du, How similar were the 1934 and 1966 Parkfield earthquakes?, *J. Geophys. Res., 98,* 4527-4538, 1993.

Segall, P., and R. Harris, Slip Deficit on the San Andreas fault at Parkfield, California, as revealed by inversion of geodetic data, *Science, 233,* 1409-1413, 1986.

Shen, Z. -K., and D. D. Jackson, GPS reoccupation of early triangulation sites: Tectonic deformation of the Southern Coast Ranges, *J. Geophys. Res., 98,* 9931-9946, 1993.

Sieh, K. E., Slip along the San Andreas fault associated with the great 1857 earthquake, *Bull. Seismol. Soc. Am., 68,* 5, 1421-1448, 1978.

Sieh, K. E., and R. H. Jahns, Holocene activity of the San Andreas fault at Wallace Creek, California, *Geol. Soc. Am. Bull., 95,* 883-896, 1984.

Sims, J. D., Geologic map of the San Andreas fault in the Parkfield 7.5-minute quadrangle, Monterey and Fresno counties, California, *U.S. Geol. Surv. Misc. Field Studies Map MF-2115,* 1990.

Toppozada, T. R., Parkfield earthquake history (abstract), *Eos Trans. AGU, 73,* Fall Meet. Suppl., 406, 1992.

Wahba, G., *Spline Models for Observational Data,* Society for Industrial and Applied Mathematics, Philadelphia, Pa., 1990.

Zumberge, J. F., M. B. Heflin, D. C. Jefferson, M. M. Watkins, and F. H. Webb, Precise point positioning for the efficient and robust analysis of GPS data from large networks, *J. Geophys. Res., 102,* 5005-5017, 1997.

J. R. Murray, P. Segall, and P. Cervelli, Department of Geophysics, Stanford University, Stanford, CA, 94305-2215, USA. (e-mail: jrmurray@stanford.edu; segall@stanford.edu; cervelli@stanford.edu)

W. Prescott and J. Svarc, United States Geological Survey, 345 Middlefield Rd., Menlo Park, CA, 94025, USA. (e-mail: prescott@usgs.gov; svarc@usgs.gov)